NMR STUDY OF DIFFUSION IN MIXTURES OF CARBON DIOXIDE AND FUNCTIONALIZED IONIC LIQUID

By

HAN WANG

A THESIS PRESENTED TO THE GRADUATE SCHOOL
OF THE UNIVERSITY OF FLORIDA IN PARTIAL FULFILLMENT
OF THE REQUIREMENTS FOR THE DEGREE OF
MASTER OF SCIENCE

UNIVERSITY OF FLORIDA

2013

To my Mom, my Dad and my Grandparents

ACKNOWLEDGMENTS

I am surrounded by people who have encouraged me during my studies at the University of Florida. First, I would like to thank Dr. Sergey Vasenkov who has provided me the opportunity to do research with his group for 2 years. It has given me a great background in research. I also want to appreciate Eric Hazalbaker who is the PhD student in Dr.Vasenkov's group that brings me great assistants no matter during measurement time or at the results discussions. I also want to thank Robert Mueller who is the other PhD student in group that are always willing to clarify my doubts during research.

Leaving motherland and perusing a degree in a foreign country is not an easy task for me. Thanks to all my family members who give me economic and spiritual support all the time especially when I was feeling frustrated by some difficulties. Thanks to Ellen who is always a good companion in my life. It is my honor to be a gator here and let's go gators!

TABLE OF CONTENTS

page

ACKNOWLEDGMENTS 4

LIST OF TABLES 6

LIST OF FIGURES 7

LIST OF ABBREVIATIONS 8

ABSTRACT 10

CHAPTER

1 INTRODUCTION 11

Transport and Diffusion 11
Diffusion Measurements by Using PFG NMR 13
Basics of NMR 13
Longitudinal and Transverse Magnetization 14
NMR Relaxation 16
Signal Detection 17
PFG NMR Stimulated Echo Pulse Sequence 18
PFG NMR Stimulated Echo Longitudinal Encode-decode Pulse Sequence 19
PFG NMR Stimulated Echo with Bipolar Gradients Pulse Sequence 20
PFG NMR Attenuation 21

2 SELF-DIFFUSION OF $^{13}CO_2$ IN TASK-SPECIFIC IONIC LIQUID 22

Introduction about Ionic Liquid 22
Results and Discussion 22
Conclusion 31

LIST OF REFERENCES 32

BIOGRAPHICAL SKETCH 34

LIST OF TABLES

Table page

1-1 Attenuation parameters in different types of pulse sequences Equations 21

2-1 Updated diffusion data acquired using τ_1 value, $\tau_1 = 0.004845s$ 29

LIST OF FIGURES

Figure		page
1-1	Spin Figure……	14
1-2	Magnezation Figure	15
1-3	Relaxation Figure	16
1-4	PFG NMR Stimulated Echo Pulse Sequence.	18
1-5	PFG NMR Stimulated Echo Longitudinal Encode Decode Pulse Sequence	19
1-6	PFG NMR Stimulated Echo Pulse Sequence with Bipolar Gradients.	20
2-1	NMR Spectrum	23
2-2	Exchange Experiment Data.	26
2-3	Attenuation Curve Data.	30
2-4	Self-Diffusivity Data.	30

LIST OF ABBREVIATIONS

FID	Free Induction Delay
MSD	Mean Square Displacement
NMR	Nuclear Magnetic Resonance
PFG NMR	Pulsed Field Gradient Nuclear Magnetic Resonance
PGSTE	PFG NMR Stimulated echo pulse sequence
PGSTE-LED	PFG NMR Stimulated echo longitudinal encode decode pulse sequence
r.f. Pulse	Radio Frequency Pulse
B_0	Amplitude of the External Static Magnetic Field
B_1	Amplitude of the Oscillating Microscope Magnetic Field due to r.f. Pulse
c	Concentration of Molecules
c^*	Concentration of Labeled Molecules
D	Diffusion Coefficient
g	Amplitude of the Magnetic Field Gradient
J	Flux of Molecules
J^*	Flux of Labeled Molecules
M	The Total Number of Diffusing Molecules
M_z	Net Total Longitudinal Magnetization
M_0	Net Total Longitudinal Magnetization at Equilibrium State
P	Distribution of Spin Phase
$\langle r^2 \rangle$	Mean Square Displacement
γ	Gyro magnetic Ratio
t	Time

τ_1	Duration between the First and Second r.f. pulses in PFG NMR Echo Longitudinal Encode Decode Pulse Sequence
τ_2	Duration between the Second and Third r.f. pulses in PFG NMR Echo Longitudinal Encode Decode Pulse Sequence
Δ	Diffusion Time
δ	Duration of the Magnetic Field Gradient Pulse
T_1	Spin-Lattice NMR Relaxation Time
T_2	Spin-Spin NMR Relaxation Time
T_{LED}	Duration between the Fourth and Fifth r.f. pulses in PFG NMR Echo Longitudinal Encode Decode Pulse Sequence for Dissipating the Eddy Current
$\hat{\mu}$	Magnetic Moment of Nuclear Spin
W_0	Larmor Frequency
Ψ	Attenuation of the Amplitude of Signal in PFG NMR Experiment
z	Position of Molecule or Spin is at z Coordinate

Abstract of Thesis Presented to the Graduate School
of the University of Florida in Partial Fulfillment of the
Requirements for the Degree of Master of Science

NMR STUDY OF DIFFUSION IN MIXTURES OF CARBON DIOXIDE AND FUNCTIONALIZED IONIC LIQUID

By

Han Wang

December 2013

Chair: Sergey Vasenkov
Major: Chemical Engineering

This thesis focuses on pulsed-field gradient nuclear magnetic resonance (PFG NMR) study of self-diffusion in mixtures of CO_2 and a task-specific ionic liquid. Complementary chemical exchange experiments performed for CO_2 provided additional information that allowed understanding and quantifying the self-diffusion data.

The thesis discusses basic background knowledge of self-diffusion and PFG NMR. Furthermore, a brief discussion of the task-specific ionic liquid will also be given. The measured PFG NMR and NMR chemical exchange data are presented and discussed. The data interpretation is provided at the end of the thesis.

CHAPTER 1
INTRODUCTION

Transport and Diffusion

One-dimensional diffusion can be described by Fick's First Law[1]:

$$J = -D\frac{\partial c}{\partial z} \tag{1-1}$$

where J is the flux of diffusing molecules/ions along the z direction, c(z) is concentration and D is the corresponding diffusion coefficient known as transport diffusion coefficient. It relates flux of molecules and concentration/chemical potential gradient under non equilibrium conditions. Assume D is independent of concentration. Then combined with mass balance we could convert Equation 1-1 to below, which is Fick's second Law of diffusion

$$\frac{\partial c}{\partial t} = \frac{\partial [D(c)\frac{\partial c}{\partial z}]}{\partial z} \tag{1-2}$$

As mentioned above that D is independent of concentration, then the Equation 1-2 could be simplified to

$$\frac{\partial c}{\partial t} = D\frac{\partial^2 c}{\partial z^2} \tag{1-3}$$

In addition to transport diffusion briefly discussed above we can also consider self-diffusion, viz. diffusion process that exists due to thermal motion of molecules even when there are no macroscopic concentration gradients and gradients of chemical potentials. It is important to note that the coefficients of transport and self-diffusion are not always the same under the same conditions.

Based on Equation 1-1, self-diffusion coefficient could be expressed under the circumstance that all the tagged molecules in system are confined to a certain region of

space at time zero when overall molecular concentration is the same. Then the Equation could be rearranged as shown below:

$$J^* = -D_{self} \left. \frac{\partial c^*}{\partial z} \right|_{c=const} \tag{1-4}$$

where, c^* is the concentration of the tagged molecules. For the case of one-dimensional diffusion with a constant diffusivity and the initial concentration of tagged molecules, the solution could be described as following:

$$c = \frac{A}{\sqrt{t}} \exp\left(\frac{-z^2}{4Dt}\right) \tag{1-5}$$

where A is the normalized constant. Fickian flux Equation for the case of three-dimensional diffusion can be presented as

$$-J_i = \sum_j D_{ij} \frac{\partial c}{\partial j} \tag{1-6}$$

Where D_{ij} is the diffusion coefficient in i direction due to concentration gradient in the j direction.

As at close system situation the total mass of diffusing species remains unchanged. Then total mass M of diffusants could be gained from corresponding concentration profiles. In a case of isotropic diffusion starting at r=0, the distribution Equation of concentration could be written

$$\frac{c}{M} = \frac{\exp\left(\frac{-r^2}{4Dt}\right)}{(4\pi Dt)^{\frac{3}{2}}} \tag{1-7}$$

Where c/M is equivalent to the diffusion progagator[2] or a probability density function P (r_2,r_1,t). Then the mean square displacement of the molecules could be gained from the variance of the Gaussian as

$$\left\langle r^2(t)\right\rangle = \int r^2 \frac{\exp(\frac{-r^2}{4Dt})}{(4\pi Dt)^{\frac{3}{2}}} dr = 6Dt \tag{1-8}$$

Diffusion studies can be achieved on many experimental techniques. However, length scale around 1 nm or similar would be too small in comparison to displacements. Pulsed field gradient NMR (PFG NMR) becomes the most capable method of collecting self-diffusion data especially coefficient.

Diffusion Measurements by Using PFG NMR

NMR stands for nuclear magnetic resonance which is a spectroscopy technique for utilizing nuclear magnetism. Its function is usually associated with atomic nuclei. Application of NMR requires knowledge of NMR background which is briefly outlined below.

Basics of NMR

Spin is a property that many atomic nuclei possess. It is also named as spin angular momentum but does not have similar characteristic like angular momentum in classical mechanics which arises from some rotational motion. Instead, it is an intrinsic property of protons and neutrons that nuclei are composed of. Its magnetic sensitivity makes it relate to the magnetic moment as the Equation shown below

$$\hat{\mu} = \gamma \hat{S} \tag{1-9}$$

where $\hat{\mu}$ is the magnetic moment and $\hat{S}$ is the spin angular momentum. γ is the gyromagnetic ratio which could be either negative or positive. The sign of γ determines

the magnetic moment being parallel or counter parallel to the direction of spin polarization.

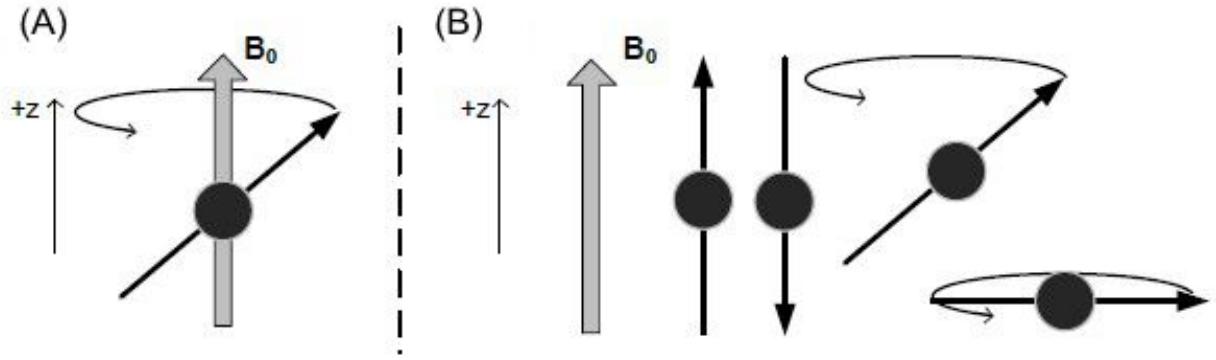

Figure 1-1 A) Schematic representation of spin precession on the presence of an external magnetic field B_0; B): Angle of precession cone depends on initial spin polarization.

In the case of no external magnetic field, spin-polarization turns to isotropic and net nuclear magnetization becomes zero. But as long as there is an external magnetic field being applied, it exerts a torque which forces the spin polarization to move on a cone always keeping the same angle between the directions of magnetic moment and the field (Fig 1-1A). This motion is known as precession (Fig 1-1B). The frequency of precession is known as as Larmor frequency. It depends on the amplitude of the magnetic field B_0 [3][4]

$$\omega_0 = -\gamma B_0 \tag{1-10}$$

where ω_0 is the Larmor frequency.

Longitudinal and Transverse Magnetization

As mentioned above, in the absence of the external field, the spin polarization is isotropic, which indicates that all the nuclei spins are pointing at random directions. In this case the net magnetization equals to zero. As long as the external magnetic field is

turned on, all the spins begin to process around the field. And eventually the spin polarization would be directed along the magnetic field direction resulting in longitudinal magnetization.

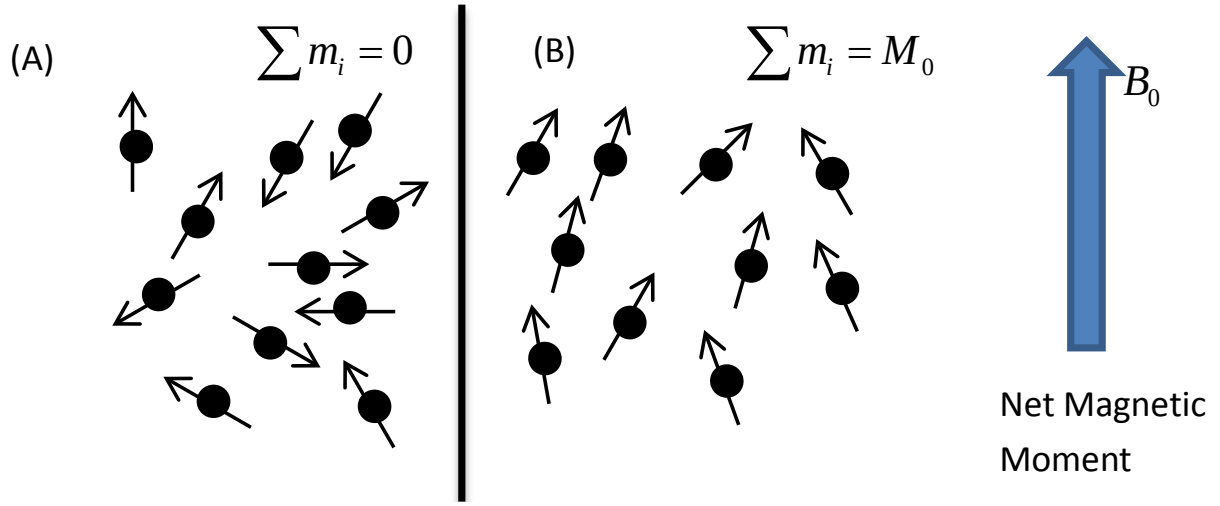

Figure 1-2 A) No magnetization in absence of external magnetic field; B) Schematic representation of longitudinal net magnetization when external magnetic field B0 is switched on. The longitudinal magnetization M0 is the vector sum of the individual magnetic moments mi [4]

Compared with other magnetization mechanisms such as electronic magnetization, bulk magnetization, the value of nuclear magnetization becomes quite small, which causes detecting the magnetization along z direction unreasonable. Another oscillating magnetic field B_1 need to be applied to make the detection more reliable. B_1 field frequency is typically in the range of radio waves. Application of this filed is referred to as an r.f. pulse. This r.f. pulse will make all the spin flip to transverse direction and makes the magnetization measurement detectable (Fig 1-3).

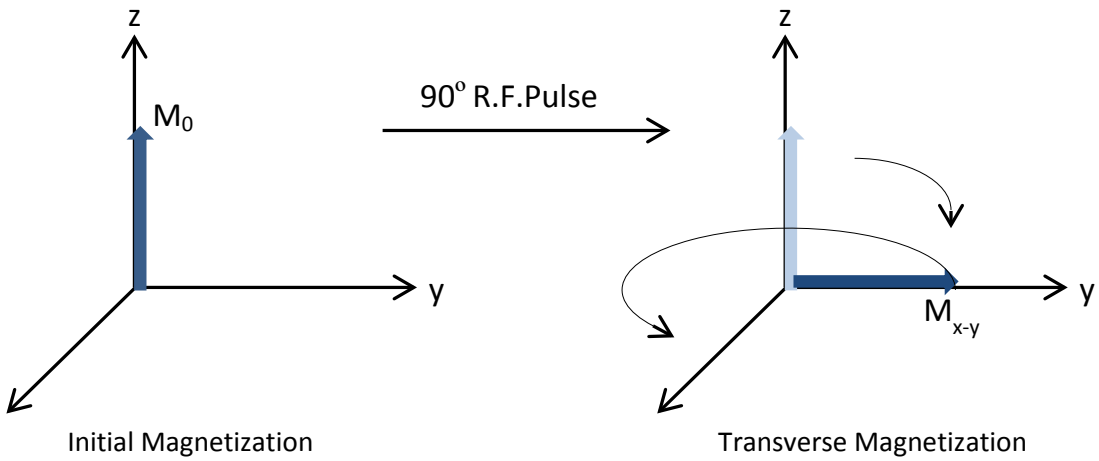

Figure 1-3 Rotation of net initial magnetization M0 oriented along +z direction, into the transverse plane by 90° r.f. pulse. The transverse magnetization Mx-y precesses in the transverse plane with Larmor frequency ω_0 [5]

NMR Relaxation

The process of the returning of the net nuclear magnetization to its equilibrium state is NMR relaxation. There are two types of NMR relaxation: (1) Spin-lattice/Longitudinal relaxation, also named as T_1 relaxation; (2) Spin-spin/transverse relaxation, also named as T_2 relaxation.[3][4][6]

T_1 relaxation is the process that deals with the gradual growth of the net nuclear magnetization back to its equilibrium value along +z direction in the presence of a B_0 field. Non-secular part of transverse relaxation would be caused along the transverse plane during the T_1 relaxation. The rate of the growth of the net magnetization along the z direction due the T_1 relaxation can be generated by the longitudinal relaxation time(T_1)

$$M_Z(t) = M_0(1 - \exp(-\frac{t}{T_1})) \qquad (1\text{-}11)$$

Where $M_Z(t)$ is the net longitudinal magnetization at time t, M_0 is the net equilibrium magnetization, which points along +z direction. The Equation 1-11 holds for the cases

when the net longitudinal magnetization is equal to zero at t=0, in presence of an external magnetic field.

As mentioned above T_2 relaxation is at when all the spins are flipped to the transverse plane, furthermore, all the spins remain in a phase coherence situation. It is caused by disturbances in local magnetic field by neighboring magnetic entities that when time goes on, various spins would de-phase and makes the net transverse magnetization gradually decay to zero. Also, the presence of fluctuation microscopic magnetic field is another reason of T_2 relaxation. The net rate of T_2 relaxation can be generated by a time constant T_2

$$M_{X-Y}(t) = M_{X-Y}(0)\exp(-\frac{t}{T_2}) \qquad (1\text{-}12)$$

where $M_{X-Y}(t)$ is the net transverse magnetization at time t.

Signal Detection

The signal detection is completed along the transverse plane. Due the re-phasing, the net magnetization would gradually decay to zero which would become an echo received by the particular coil installed in the spectrometer. The decay is known as free induction decay(FID). With the application of Fourier transformation, FID data would be collected as NMR spectra.

Though in an external magnetic field B_0, all the atomic nuclei of a certain type should be the same and equal to Larmor frequency. In facts, some deviations would occur due to chemical shift. It is a consequence of slight variations in the effective field experienced by a nucleus because of the local atomic environment. Chemical shift in ppm units could be calculated as

$$\delta^* = \frac{\omega - \omega_{ref}}{\omega_{SF01}} \tag{1-13}$$

where δ^* is the chemical shift in ppm, ω is the measured frequency, ω_{ref} is the reference frequency and ω_{SF01} is Carrier Frequency known as the operating frequency of the magnet. The use of ppm scale greatly simplifies the comparison of data acquired at different amplitudes of the constant magnetic field.

PFG NMR Stimulated Echo Pulse Sequence

PFG NMR makes use of the dependence of Larmor frequency on the applied constant magnetic field. In PFG NMR a gradient of magnetic field along the z direction is applied that labels the nuclear spins based on their spatial positions along the z direction

$$\omega = -\gamma(B_0 + gz) \tag{1-14}$$

Where ω is the Larmor frequency, γ is the gyromagnetic ratio, B_0 is the external magnetic field, g is the linear gradient of the magnetic field applied on transverse field.

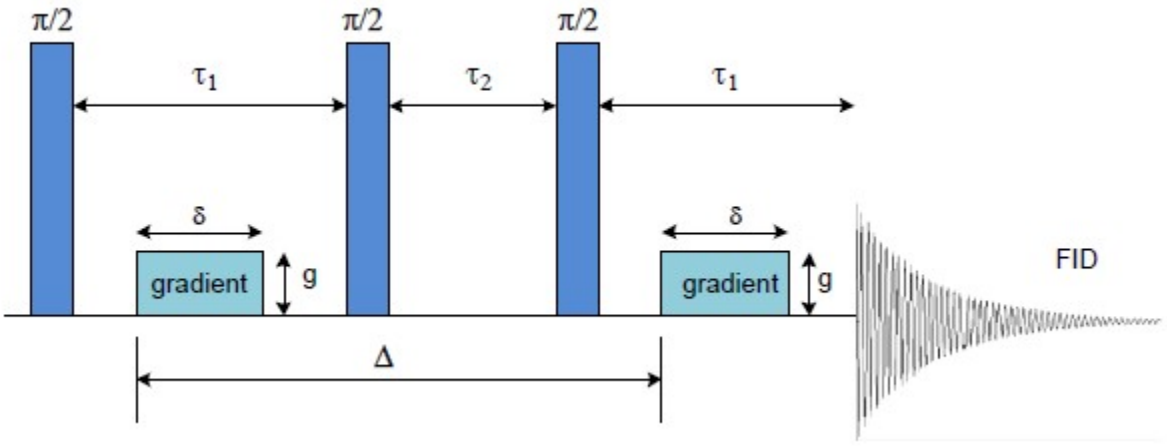

Figure 1-4 Schematic of PFG NMR simulated echo pulse sequence. This sequence is of great advantage for systems in which the T2 NMR relaxation time is much shorter than T1 NMR relaxation time.

Fig 1-4 indicates the schematic of PFG NMR simulated echo pulse sequence. It is made of three $\frac{\pi}{2}$ pulses and two field gradient of identical amplitude g and duration δ. The first r.f. pulse is the one that flipped the spins and make longitudinal magnetization to the transverse plane and the first gradient is to tag the spins precessing with different Larmor frequency and de-phasing. The time interval τ_1 is the de-phasing interval. Then the second r.f. pulse is to tilted the spins to the –z direction and the third one is to flipped the spins back to the transverse plane. And the time interval Δ refers to the measuring diffusion time. If diffusion happens during the Δ time interval, then the de-phasing will not be completed and there would a decrease of the intensity amplitude.

This pulse sequence is very useful for the situation when the product's T_1 value is larger than its T_2 value.

PFG NMR Stimulated Echo Longitudinal Encode-decode Pulse Sequence

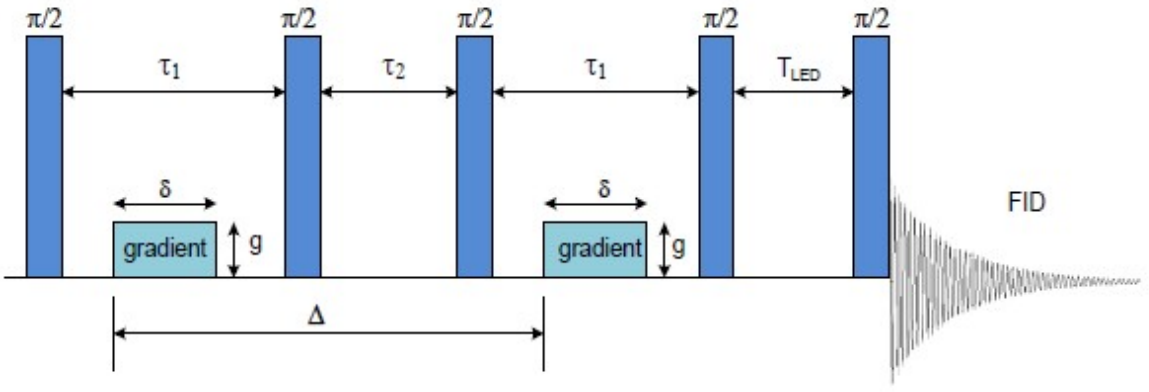

Figure 1-5 Schematic of the PFG NMR stimulated echo longitudinal encode decode pulse sequence.

PFG NMR stimulated echo longitudinal encode decode pulse sequence is basically applied when eddy current, which in the coil that causes inhomogeneity in the

magnetic field, needs to be avoided to get clear data. This method is also known as longitudinal eddy current delay pulse sequence (PGSTE-LED)[7]. There are two more r.f. pulses compared with simulated echo pulse sequence. And the extra two r.f. pulses could be seen that are applied at the very end of the sequence which is to eliminate the eddy current.

This sequence could be applied when T_2 is very small so increasing the time interval would affect the signal produced by T_2. During T_{LED} time only T_1 affect the signal reception so which could easily help to divide the affection of both T_1 and T_2.

PFG NMR Stimulated Echo with Bipolar Gradients Pulse Sequence

This pulse sequence is also known as the 13-interval sequence.[8]-[11]The advantage of this pulse sequence is that it could eliminate the background gradients produced by some heterogeneous media.

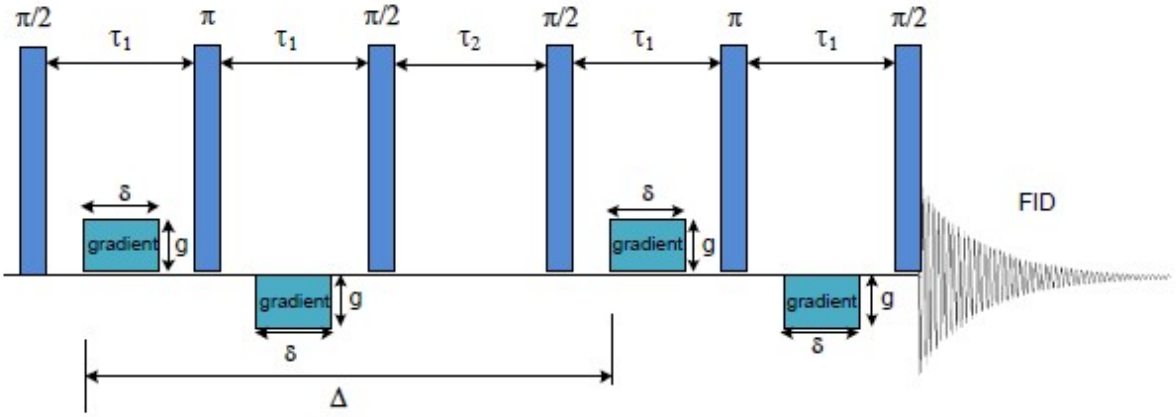

Figure 1-6 Schematic of the PFG NMR stimulated echo pulse sequence with bipolar gradients. Bipolar Gradients are used to suppress internal gradients.

This stimulated echo pulse sequence with bipolar gradients introduces two negative r.f. pulses right after another pulse which is to help get rid of the background gradients.

PFG NMR Attenuation

Dependence of the attenuation of the PFG NMR signal Ψ on the amplitude *g* of the applied field gradient allows obtaining molecular diffusivities. The general form of attenuation Equation for normal isotropic diffusion is

$$\psi(\delta g.t_{eff}) = \exp(-(k)^2 D t_{eff}) \tag{1-15}$$

The table 1-1 below gives the parameter expression at each different types of pulse sequences.

Table 1-1 Attenuation parameters in different types of pulse sequences Equations

Sequence Type	PGSTE/PGSTE-LED	t_{eff} 13-interval sequence
k	$\gamma g \delta$	$2\gamma g \delta$
t_{eff}	$\Delta - \frac{\delta}{3}$	$\Delta - \frac{\tau}{2} - \frac{\delta}{6}$

In case when several molecular ensembles with different diffusivities contribute to the measured PFG NMR signal Eq. 1-15 needs to be modified as follows

$$\psi(\delta g.t_{eff}) = \sum_i^n p_i \exp(-(k)^2 D_i t_{eff}) = \sum_i^n p_i \exp(-(k)^2 \frac{\left\langle r_i^2(t_{eff}) \right\rangle}{6} \tag{1-16}$$

where p_i refers to the fraction of molecules diffusing with the Diffusivity constant D_i.

CHAPTER 2
SELF-DIFFUSION OF $^{13}CO_2$ IN TASK-SPECIFIC IONIC LIQUID

Introduction about Ionic Liquid

It is essential to find applicable liquid adsorbent for CO_2 capture. Ionic liquids, molten salts that are liquid at temperatures around room temperature, show many useful properties including negligible vapor pressure and high thermal stability which make these liquids promising sorbents for CO_2 capture .[12] Chemical modification of an ionic liquid consisted of an attachment of an amine group to the cation has been determined to result in highly selective and reversible capture of CO_2.[13-16]

This task-specific ionic liquids (TSIL) used as CO_2 absorbents has an disadvantage of high viscosity [13] which can lead to transport limitations in the process of CO_2 absorption. The main focus of this thesis is to find out the relationship between CO_2 diffusion and the process of CO_2 exchange between the chemically-bound, viz. chemisorbed, and physisorbed states in the mixture of CO_2 and the TSIL. The TSIL chosen for these studies is composed of $(CH_3)_3N(CH_2)_2NH_2^+$ cation and $(CF_3SO_2)_2N^-$ anion. The expected stoichiometric reaction of CO_2 with this TSIL is given by the following Equation

$$2(CH_3)_3N(CH_2)_2NH_2^+ + 2(CF_3SO_2)_2N^- + CO_2 \rightleftharpoons (CH_3)_3N(CH_2)_2NH_3^{2+} + CH_3)_3N(CH_2)_2NHCOO + 2(CF_3SO_2)_2N^-, \quad (2\text{-}1)$$

where the first and second species on the right-hand part are dication and zwitterion.

Results and Discussion

Figure 2-1 shows examples of the ^{13}C NMR spectra obtained by a one pulse sequence for pure TSIL of $[(CH_3)_3N(CH_2)_2NH_2]^+$ and $[CF_3SO_2)_2N]^-$ and a mixture of TSIL $[(CH_3)_3N(CH_2)_2NH_2]^+[CF_3SO_2)_2N]^-$ and CO_2. In the $[(CH_3)_3N(CH_2)_2NH_2]^+[CF_3SO_2)_2N]^-$

spectrum (Fig. 2-1A) the quartet centered at around 120 ppm originate from the anion, with the rest of the lines originating from the cation. Compared with the pure TSIL spectrum, there are two more additional lines at around 161 and 125 ppm appeared in the mixture sample which refers to the CO_2 peaks. The chemical shift of the former line corresponds to the known chemical shift of the carbonate group ($HN_{13}C(O)O^-$) [17,18]. Hence, this line can be assigned to chemisorbed CO_2. The line at around 125 ppm originates from physisorbed CO_2. The lines at around 161 and 125 ppm were used to study diffusion and chemical exchange of CO_2. The strongest anion lines at 119 and 120 ppm were used for determining the anion diffusivity. The cation diffusivity was obtained using the strongest overlapping cation lines at around 53 ppm. The diffusivities is gained from 3-5 repeating steps of the average attenuation curve measurement.

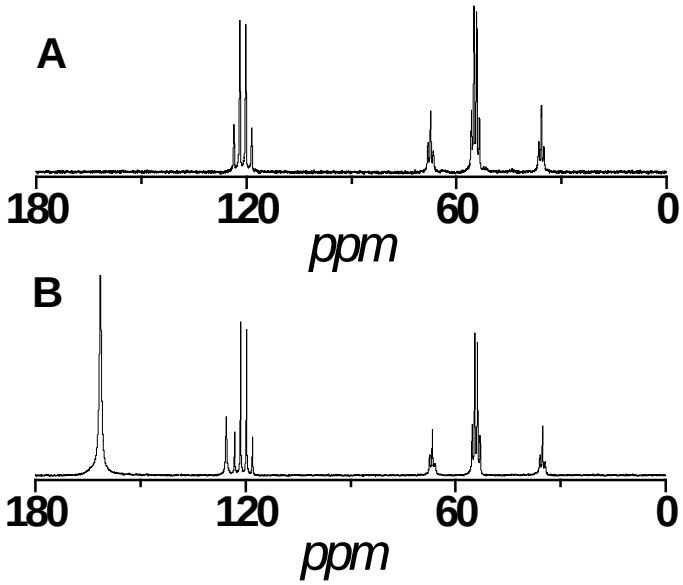

Figure 2-1 A) NMR spectrum pure TSIL; B) NMR spectrum of that containing 0.06 $^{13}CO_2$ molecules per anion-cation pair. The spectra were recorded by a ^{13}C NMR one-pulse sequence. The chemical shifts are referenced to a doped dioxane in benzene standard.[19]

The exchange of CO_2 between the chemisorbed and physisorbed states is performed by applying a sequence of ^{13}C NMR exchange experiments (EXSY). One-dimensional (1D) EXSY sequence (selective $\pi/2$) - $\pi/2$ - τ_{mix} - $\pi/2$ - Acquisition[20,21] with a selective excitation pulse being used because of being compared with 2D it is more efficient and simpler [20-23]. 1D EXSY measurements result can be viewed as relaxation-type experiments where the selective $\pi/2$ pulse was applied for the on-resonance spins of physisorbed carbon dioxide and the NMR signals of both chemisorbed and physisorbed CO_2 were monitored as a function of the mixing time τ_{mix}. To separate the effects of longitudinal T1 relaxation from the effects of chemical exchange during mixing time the standard inversion recovery (IR) measurements were also performed. Fig. 2-2 shows the results of 1D EXSY and inversion recovery measurements. The data in Fig.2-2 indicate that while the normalized signals measured by the 1D EXSY sequence experience an order of magnitude change when the mixing time is increased from around 0 to 0.03 s, the corresponding normalized signals measured by the IR sequence remains essentially fixed for the same mixing time range. Hence, it can be concluded that the chemical exchange revealed by the 1D EXSY experiment occurs on a much shorter time scale than the T1 relaxation. Simplifying analysis of the exchange data could be achieved from the results. In particular, the mean residence time of CO_2 in the physisorbed state can be estimated from the initial slope of the decay of the signal at 125 ppm shown in Fig. 2-2 B using [24]

$$I_{phys}(\tau_{mix}) = I_{phys}(0)\exp(-\tau_{mix}/t_{phys}) \qquad (2\text{-}2)$$

where I_{phys} is the intensity of the normalized signal at 125 ppm and t_{phys} is the mean residence time in the physisorbed state. This Equation is expected to hold for

sufficiently small values of the mixing time corresponding to $\frac{I_{phys}(\tau_{mix})}{I_{phys}(0)} \leq 0.4$ when it can be assumed that the contribution to I_{phys} of the CO_2 molecules that experienced the transition from the physisorbed to chemisorbed state, and then back to the physisorbed state is negligibly small [24]. This assumption is justified by the observation that the equilibrium population of the chemisorbed state is around 8.7 times larger than that of the physisorbed state, as revealed by the ratio of the CO_2 line intensities at 125 and 156 ppm in Fig. 1-1 B. Hence, for the considered range of small mixing times corresponding to $\frac{I_{phys}(\tau_{mix})}{I_{phys}(0)} \leq 0.4$ a vast majority of the molecules in the chemisorbed state are expected to be those that also were there at $\tau_{mix} = 0$. Obviously, these molecules make great contributions to the transition from chemisorbed to physisorbed . Best fit of the initial portion of the 1D EXSY decay curve in Fig. 2-2B to Eq. 2-2 yields $t_{phys} \approx 8.8ms$.

The mean residence time in the chemisorbed state (t_{chem}) can be estimated by taking into account that for a two-state exchange the ratio of the equilibrium populations of molecules in the two states is equal to the corresponding ratio of the mean residence times. Then it could be easily determined that the mean residence time of chemisorbed by multiple the value of physisorbed mean residence time of 7.6 times as mentioned above. $t_{chem} \approx 76ms$.

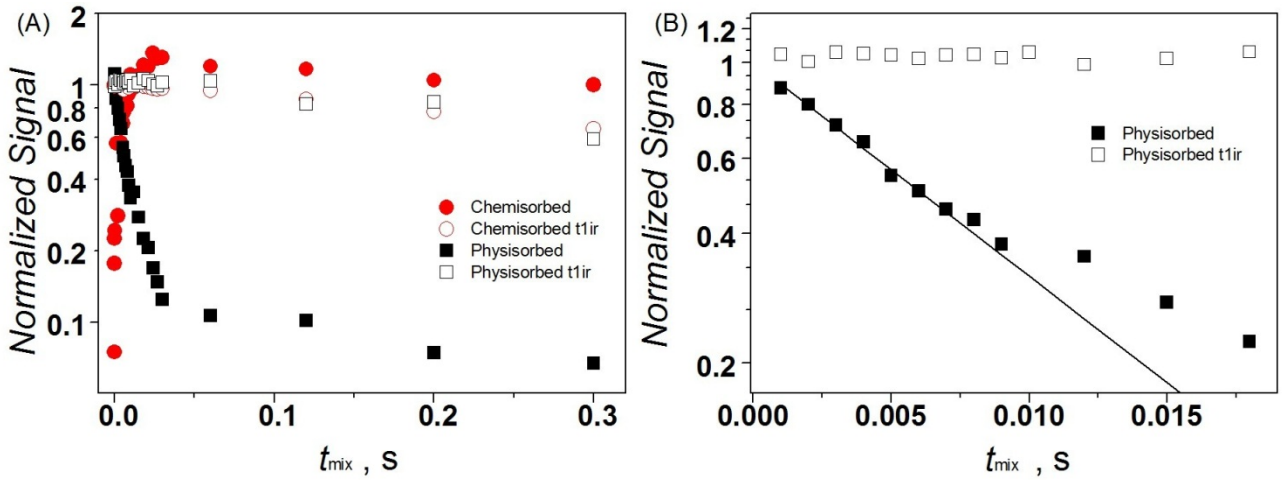

Figure 2-2 A) Results of 13C NMR selective 1D EXSY experiments where the selective $\pi/2$ pulse was applied for the on-resonance spins of the physisorbed carbon dioxide at 125 ppm. Also shown for comparison are the corresponding data obtained by a standard inversion recovery (IR) pulse sequence.
B) The same data for the line of the physisorbed carbon dioxide at 125 ppm but zoom in at smaller time scale. Solid line shows the best fit of the exchange data at small mixing times of Eq. 2-2.

^{13}C PFG NMR diffusion measurements for the ions and CO_2 were performed using the standard stimulated echo PFG NMR sequence $\pi/2$ - τ_1 - $\pi/2$ - τ_2 - $\pi/2$ - τ_1 - Acquisition as mentioned in Chapter 1. The measurements were carried out for the effective diffusion times comparable with and much larger than the values of the mean residence times of CO_2 molecules in the physisorbed and chemisorbed states (t_{phys} and t_{chem}). It was not technically possible to perform ^{13}C PFG NMR studies for diffusion times smaller than t_{phys}. Due to the signal-to-noise limitations in the PFG NMR measurements the maximum signal attenuation by diffusion did not accede 65-70% of the total signal at zero or small gradient strength. It was observed that the measured attenuation curves in all cases did not show any significant deviations from the monoexponential behavior expected for normal diffusion with a single diffusivity. Fig.2-3 shows examples of the measured attenuation curves for the ion lines discussed above as well as for CO_2 lines at 156 and 125 ppm. When

performing diffusion measurements under the conditions of chemical exchange special care must be taken when choosing the duration of the time interval τ_1 of the stimulated echo PFG NMR sequence to make the mean residence time of exchange negligible. The choice of this time interval is important because the contribution of CO_2 molecules that were in different states during the first and second time interval τ_1 of the sequence to the measured signal is expected to be proportional to cos($\Delta\omega\tau_1$), where $\Delta\omega$ is the difference between the precession frequencies in the chemisorbed and physisorbed states [25]. Under experimental conditions the existence of such dependence was confirmed by performing measurements with the PFG NMR stimulated echo sequence at a fixed, small gradient strength. The measurements were carried out with different values of τ_1 chosen such that the probed range of the values of $\Delta\omega\tau_1$ covered around 3π for each diffusion time used. The PFG NMR diffusion data reported were obtained under conditions when cos($\Delta\omega\tau_1$) = 1. This corresponds to the situation when the spins that were in different chemical environments during the first and second time interval τ_1 of the sequence fully contribute to the measured signal. An analytical solution for this case is presented in Refs. [26,27] With Equations below

$$M_A = [\frac{M_{A0}}{2} - \frac{(\delta M_{A0} - k_B M_{B0})}{2\Delta}]\exp[(-\sigma + \Delta)T] + [\frac{M_{A0}}{2} - \frac{(\delta M_{A0} - k_B M_{B0})}{2\Delta}]\exp[(-\sigma - \Delta)T]$$
$$M_B = [\frac{M_{B0}}{2} - \frac{(\delta M_{B0} - k_A M_{A0})}{2\Delta}]\exp[(-\sigma + \Delta)T] + [\frac{M_{B0}}{2} - \frac{(\delta M_{B0} - k_A M_{A0})}{2\Delta}]\exp[(-\sigma - \Delta)T] \quad \text{(2-3A,B)}$$

where M_A is the species physisorbed CO_2 “on-resonance” nuclear magnetization and k_B is the rate constant of species chemisorbed CO_2, with

$$\sigma = \frac{1}{2}[k_A + k_B + D_A K^2 + D_B K^2]$$

$$\delta = \frac{1}{2}[k_A - k_B + D_A K^2 - D_B K^2]$$

$$\Delta = \sqrt{\delta^2 + k_A k_B}$$

And D_A is the diffusion constant of species physisorbed CO_2.

It is important to note that this solution was developed for the measurement conditions when NMR relaxation effects can be neglected. It was observed that in agreement with this solution the effective diffusivities given by the initial slopes of the measured attenuation curves for the CO_2 lines at 125 and 156 ppm are different at short diffusion times and approach the same diffusivity with increasing diffusion time (Fig.2-4). For the largest diffusion time of 1.2 s both diffusivities are the same within the experimental uncertainty indicating that the condition of fast exchange of CO_2 molecules between the chemisorbed and physisorbed states is reached for this diffusion time. Fitting the initial parts of the carbon dioxide PFG NMR attenuation curves to Eqs. 2-3A and 2-3B for the effective diffusion times between 0.03s and 1.2s allowed estimating the diffusivities of the chemisorbed and physisorbed carbon dioxide. For these times only the initial parts of the attenuation curves ($\Psi \leq 0.7$) were used in the fit to reduce an influence of NMR relaxation, which can change the shape of the measured PFG NMR curves, but is not taken into account in the derivation of Eqs. 2-3A and 2-3B. For the largest diffusion time of 1.2 s the attenuation curves predicted by Eqs. 2-3A and 2-3B are monoexponential in agreement with the experimental observation. In this case the fitting was performed for the whole measured attenuation curves. The resulting CO_2 diffusivities in the physisorbed and chemisorbed states are shown in Table 2-1 together with the ranges of diffusion times used to obtain the diffusion data.

Table 2-1 Updated diffusion data acquired using τ_1 value, $\tau_1 = 0.004845s$.

Diffusion Time , s	Physisorbed CO_2 Diffusivity x 10^{-12} , m^2s^{-1}	Chemisorbed CO_2 Diffusivity x 10^{-12} , m^2s^{-1}
0.03	16.1 ± 3.2	2.7 ± 0.5
0.04	13.6 ± 2.7	3.7 ± 0.7
0.16	11.4 ± 2.3	4.4 ± 0.9
0.64	8.8 ± 1.8	4.8 ± 1.0
1.2	4.7 ± 0.9	4.2 ± 0.8

Fig.2-4 and Table 2-1 show the cation and anion diffusivities obtained from fitting the measured PFG NMR attenuation curves by Eq. 2-2. It is seen that within the experimental uncertainty the ion diffusivities in the samples with and without CO_2 are the same (Table 2-1) and do not depend on diffusion time (Fig.2-4). These results can be understood by noting that in the sample with CO_2 the number of CO_2 molecules is several times smaller than the number of the anion-cation pairs. Hence, the measured ion diffusivities, which were obtained from a relatively small PFG NMR attenuation range reflecting the diffusion behavior of the majority of ions in the sample, are not expected to be very different in the samples with and without CO_2 or to show any dependence on diffusion time.

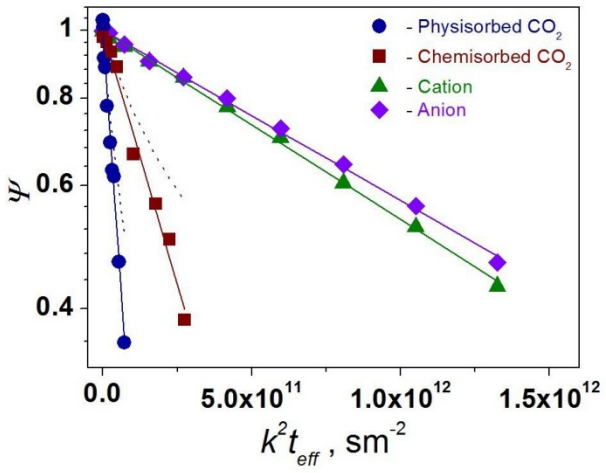

Figure 2-3 ^{13}C PFG NMR attenuation curves obtained by the ^{13}C PFG NMR STE sequence for the mixture of $[(CH_3)_3N(CH_2)_2NH_2]^+[CF_3SO_2)_2N]^-$ with CO_2 for t_{eff} ≈ 40 ms at 297 K. The attenuation curve for the anion was obtained by averaging the attenuation curves measured for the NMR lines of the anion at 122 ppm and 120 ppm. The attenuation curve for the cation corresponds to the cation line at 54 ppm. The attenuation curve for chemisorbed CO_2 corresponds to the line at 161 ppm. The attenuation curve for physisorbed CO_2 corresponds to the line at 125 ppm.

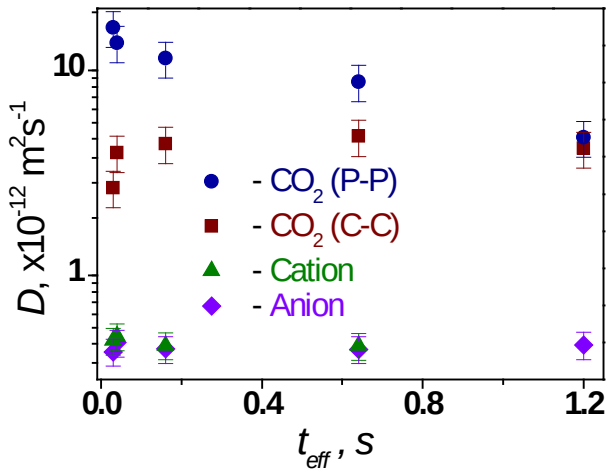

Figure 2-4 Dependence of the self-diffusivity of the cation, anion, chemisorbed CO_2, and physisorbed CO_2 to the diffusion time at 297 K. The data were obtained by ^{13}C PFG NMR.

Conclusion

This is the first time observation of chemical exchange in real ^{13}C system in the mixtures of carbon dioxide and task-specific ionic liquid. The PFG NMR measurement on diffusion of chemical exchange of CO_2 in this ^{13}C system shows the evidence and species diffusivities. The analytical solution applied with Equation 2-3A, B also correspond well to the initial slope of the experimental attenuation data. It shows that chemical exchange phenomenon can affect the diffusivity of the species of physisorbed and chemisorbed CO_2 in certain effective diffusion time range which needs to be taken into account for further diffusion study.

LIST OF REFERENCES

1. Fick, A. E. Ann. Phys. **1855**, 94, 59.

2. Auerbach S M, Kärger J, Vasenkov S. *Diffusion in zeolites*. Marcel Dekker Inc.: New York, **2003**.

3. Levitt, M. H. *Spin dynamics : basics of nuclear magnetic resonance*, 2nd ed.;John Wiley & Sons: Chichester, England ; Hoboken, NJ, **2008**.

4. Keeler, J. *Understanding NMR spectroscopy*, 2nd ed.; John Wiley and Sons: Chichester, **2010**.

5. Menjoge, Amrish Ramesh. Relationship between diffusion and structure in selected nanostructured systems by NMR. **2010**.

6. Callaghan, P. T. *Principles of nuclear magnetic resonance microscopy*; Clarendon Press Oxford University Press: Oxford England New York, **1991**.

7. Gibbs, S. J.; Johnson, C. S. *Journal of Magnetic Resonance* (1969) **1991**, 93, 395.

8. Cotts, R. M.; Hoch, M. J. R.; Sun, T.; Markert, J. T. *J. Magn. Reson*. **1989**, 83, 252.

9. Galvosas, P.; Stallmach, F.; Seiffert, G.; Kärger, J.; Kaess, U.; Majer, G. *J. Magn. Reson*. **2001**, 151, 260.

10. Wu, D. H.; Chen, A. D.; Johnson, C. S. *Journal of Magnetic Resonance, Series A* **1995**, 115, 260.

11. Wider, G.; Dotsch, V.; Wuthrich, K. *Journal of Magnetic Resonance, Series A* **1994**, 108, 255.

12. Wasserscheid, P.; Welton, T. *Ionic Liquids in Synthesis, 2nd ed.* Wiley VCH: Weinheim, **2007.**

13. Bates, E.D.; Mayton, R.D.; Ntai, I.; Davis, J.H. CO_2 Capture by a Task-Specific Ionic Liquid. *Journal of the American Chemical Society* **2002**, 124, 926-927.

14. Bara, J.E.; Camper, D.E.; Gin, D.L.; Noble, R.D. Room-Temperature Ionic Liquids and Composite Materials: Platform Technologies for CO_2 Capture. *Accounts of Chemical Research* **2009**, 43, 152-159.

15. Yang, Z.-Z.; Zhao, Y.-N.; He, L.-N. CO_2 chemistry: task-specific ionic liquids for CO2 capture/activation and subsequent conversion. *RSC Advances* **2011**, 1, 545-567.

16. Wu, C.; Senftle, T.P.; Schneider, W.F. First-principles-guided design of ionic liquids for CO_2 capture. *Physical Chemistry Chemical Physics* **2012**, 14, 13163-13170.

17. Xu, H.; Rudkevich, D.M. Controlling Capture and Release of Guests from Cross-Linked Supramolecular Polymers. *Organic Letters* **2005**, 7, 3223-3226.

18. Stastny, V.; Anderson, A.; Rudkevich, D.M. Supramolecular Structures from Lysine Peptides and Carbon Dioxide. *The Journal of Organic Chemistry* **2006**, 71, 8696-8705.

19. Gottlieb, H.E.; Kotlyar, V.; Nudelman, A. NMR Chemical Shifts of Common Laboratory Solvents as Trace Impurities. *The Journal of Organic Chemistry* **1997**, 62, 7512-7515.

20. Kessler, H.; Oschkinat, H.; Griesinger, C.; Bermel, W. Transformation of homonuclear two-dimensional NMR techniques into one-dimensional techniques using Gaussian pulses. *Journal of Magnetic Resonance* (1969) **1986**, 70, 106-133.

21. Kessler, H.; Mronga, S.; Gemmecker, G. Multi-dimensional NMR experiments using selective pulses. *Magnetic Resonance in Chemistry* **1991**, 29, 527-557.

22. Bain, A.D.; Cramer, J.A. Slow Chemical Exchange in an Eight-Coordinated Bicentered Ruthenium Complex Studied by One-Dimensional Methods. Data Fitting and Error Analysis. *Journal of Magnetic Resonance*, Series A **1996**, 118, 21-27.

23. Bain, A.D. Chemical exchange in NMR. *Progress in Nuclear Magnetic Resonance Spectroscopy* **2003**, 43, 63-103.

24. Forsen, S.; Hoffman, R.A. Study of Moderately Rapid Chemical Exchange Reactions by Means of Nuclear Magnetic Double Resonance. *The Journal of Chemical Physics* **1963**, 39, 2892-2901.

25. Chen, A.; Johnson, C.S.; Lin, M.; Shapiro, M.J. Chemical Exchange in Diffusion NMR Experiments. *Journal of the American Chemical Society* **1998**, 120, 9094-9095.

26. Johnson, C.S. Effects of Chemical Exchange in Diffusion-Ordered 2D NMR Spectra. *Journal of Magnetic Resonance*, Series A **1993**, 102, 214-218.

27. Cabrita, E.J.; Berger, S.; Bräuer, P.; Kärger, J. High-Resolution DOSY NMR with Spins in Different Chemical Surroundings: Influence of Particle Exchange. *Journal of Magnetic Resonance* **2002**, 157, 124-131.

BIOGRAPHICAL SKETCH

Han Wang was born in 1989 at Ruian, China to Lingli Zhang and Beijiao Wang. He grew up with his parents. All his early schooling was done in Ruian itself. And after junior high school he moved to Shanghai Fuxing senior high school. He finished up his bachelor degree in South China University of Technology in Guangzhou, China. He attended the University of Florida and obtained his Master of Science in chemical engineering.